

ADSORPTION OF H₂O ON CLEAN AND OXYGEN-PREDOSED Ni(110)

Carsten BENNDORF* and Theodore E. MADEY

Surface Science Division, National Bureau of Standards, Gaithersburg, MD 20899, USA

Received 4 May 1987; accepted for publication 24 August 1987

The adsorption of H₂O on both clean and modified Ni(110) surfaces has been studied using a variety of methods: electron stimulated desorption ion angular distribution (ESDIAD), thermal desorption spectroscopy (TDS), and low energy electron diffraction (LEED). Fractional monolayers, $\theta(H_2O) < 0.5$, of H₂O on clean Ni(110) are associated with a four-spot ESDIAD pattern suggesting that the H-ligands are in specific registry with the substrate. We postulate the formation of H₂O dimers bound via oxygen lone pair orbitals to Ni substrate atoms and oriented with the O ··· H–O axis in [001] azimuthal directions. For $\theta(H_2O) > 0.5$ –1 larger hydrogen bonded clusters with long range c(2 × 2) symmetry are formed. Upon heating to > 200 K, a fraction of the H₂O dissociates, forming OH(ad). TDS of H₂O from clean Ni(110) reveals four binding states having peak temperatures of 155, 210, 245 and 370 K. They are related to multilayer desorption (155 K), desorption from larger bilayer clusters (210 K), desorption from H₂O dimer clusters which might be stabilized by OH (245 K), and recombination of OH to yield H₂O(g) (360 K). Dissociation of H₂O is promoted by surface oxygen. For the adsorption of H₂O on oxygen-dosed Ni(110) at $\theta(O) > 0.08$, a mixture of molecular and dissociative adsorption occurs immediately at 80 K, producing inclined OH. Isotopic exchange of H₂¹⁶O with ¹⁸O(ad) is observed even for binding states in which dissociation is believed not to occur and is related to a proton exchange involving H₂O($\varepsilon\downarrow$) hydrogen bonded to O(ad).

1. Introduction

Recently there has been a growing interest in the study of H₂O adsorption on transition metals [1]. The molecular structure of chemisorbed H₂O, its reactivity with the clean metal surface, and the influence of surface “additives” (fractional monolayers of impurity atoms) are of fundamental interest in catalysis, electrochemistry and corrosion. On several close-packed transition metal surfaces, including Ni [2–4], Cu [5,6], Ru [7–9], Pt [10–12], Ag [13–15]

* Permanent address: Department of Physical Chemistry, University of Hamburg, Fed. Rep. of Germany.

and Re [16], H₂O is molecularly adsorbed at low temperature with evidence for bonding via the oxygen atom. Due to attractive hydrogen bonding interactions between neighboring chemisorbed H₂O molecules the *formation of H₂O clusters* even at fractional monolayer coverages has been reported for several H₂O/metal systems. Evidence for such attractive lateral interactions has been obtained from EELS (electron energy loss spectroscopy) [17], ESDIAD (electron stimulated desorption ion angular distributions) [1,2,9,12] and TDS (thermal desorption spectroscopy) [2,9].

Thermal desorption experiments for H₂O from differently oriented Ni surfaces indicate an influence of the substrate geometry on the H₂O-substrate binding energy. The peak temperature for the highest desorption state of molecular H₂O is reported to be at ~ 170 K on Ni(111), ~ 194 K on Ni(100) (with small amounts of H₂O desorbing up to 255 K [3]) and ~ 350 K on Ni(110) [4,18]. We will show that this crystallographic specificity is associated with higher reactivity of Ni(110), where a fraction of the H₂O dissociates. The substrate geometry may influence not only the binding energy but also the orientation and the formation of chemisorbed H₂O monomers and clusters. Furthermore, as pointed out by Doering and Madey [9] (hereafter: DM) the desorption temperatures for chemisorbed H₂O itself may be related to the formation or the absence of oriented clusters.

The first aim of the present work is to provide further information about the influence of substrate geometry on the structure and chemistry of chemisorbed H₂O on the Ni(110) surface.

The experimental methods include ESDIAD, LEED and TDS. Our ESDIAD results for fractional monolayer coverages suggest the formation of *H₂O dimers* at $\theta(\text{H}_2\text{O}) < 0.5$. At higher H₂O coverages, $\theta(\text{H}_2\text{O}) > 0.5$, ESDIAD and LEED indicate the formation of an *ordered H₂O bilayer* with both short and long range order. For both structures (H₂O dimers and H₂O bilayer) structural models are proposed, which are in good accordance with the Bernal–Fowler–Pauling rules [19] for ice structures, modified for chemisorbed H₂O by DM [9]. A short paper describing evidence for the existence of dimers based on ESDIAD and angle resolved ultraviolet photoemission spectroscopy has already appeared [20], and serves as a basis for the present work.

The second aim of our present work is to characterize the role of surface impurity atoms (oxygen) on the structure and reactivity of chemisorbed H₂O on Ni(110). Madey and Netzer reported that preadsorbed oxygen on Ni(111) can induce a high degree of azimuthal order in chemisorbed H₂O, whereas on the clean Ni(111) surface local azimuthal order is absent [2]. ESDIAD and TDS revealed strong interactions between H₂O(ad) and O(ad) which were suggested to be due to hydrogen bonding. In contrast to this oxygen-induced local azimuthal ordering on Ni(111), DM [9] found an ordered chemisorbed H₂O bilayer on clean Ru(001) for which the order was *destroyed* by low

coverages of preadsorbed oxygen. Evidence for the induction of steric effects (inclination of the molecular axis) in the presence of adsorbed Na was reported by Doering et al. for $H_2O/Ru(001)$ [22].

For $H_2O + O/Ni(110)$ we find evidence for a strong lateral interaction between surface oxygen and chemisorbed H_2O that can lead to dissociation of H_2O . The dissociation probability depends on both additive coverage and surface temperature. A partial account of the $H_2O + O$ results, in which hydrogen abstraction to form "inclined" OH on Ni(110) was reported, has already appeared [23].

2. Experimental procedures

The experiments were performed in an ultrahigh vacuum system equipped with facilities for AES (Auger electron spectroscopy), ESDIAD, LEED and TDS; details of the apparatus and the methods used have been described previously [24–26]. The Ni(110) single crystal was mounted on an xyz-rotary manipulator. The crystal temperature could be controlled continuously from 80 to 1000 K, and was measured with a W-5%Re/W-26%Re thermocouple spot-welded to the backside of the crystal. Cleaning of the Ni(110) crystal was achieved with repeated cycles of Ar-ion sputtering and annealing. The residual carbon could be removed by oxygen dosing followed by heating. Cleanliness and orientation were probed with AES and LEED. After cleaning, the AES intensities of possible surface contamination (i.e. S, C and O) were always below 1/50 of the Ni Auger peak intensity at 103 eV (corresponding to an impurity coverage below 1% of a monolayer).

ESDIAD and LEED patterns were viewed directly on a fluorescent screen following image-amplification of the desorbing ion (or diffracted electron) signal using a double microchannel plate detector in a retarding grid analyzer apparatus [26]. The ESDIAD patterns were compressed for viewing by applying a positive bias potential to the Ni(110) crystal. The excitation energy (sum of electron gun energy and sample bias potential) for ESD studies was 350 eV. The angle between incident electrons and the surface normal was about 50° for ESD and LEED.

Thermal desorption spectra as well as ion desorption in ESD experiments were analyzed with a quadrupole mass spectrometer (QMS). The heating rates for the TDS spectra were about 8 K/s. H_2O was dosed onto the Ni(110) crystal using a molecular beam doser with a microcapillary array as an effusion source. Oxygen was introduced to the chamber by a UHV leak valve. The amount of predosed oxygen was determined with AES using a calibration method for the O(KLL) intensity described in ref. [27].

3. Results

3.1. H_2O adsorption on clean Ni(110) at 80 K: thermal desorption spectra

Fig. 1 shows a series of thermal desorption spectra from H_2O adsorbed on clean Ni(110) at 80 K. We note with increasing H_2O exposure a sequential filling of different desorption peaks denoted as B (peak temperature $T_m = 350\text{--}360$ K), A_1 ($T_m \approx 270$ K), A_2 ($T_m \approx 210$ K) and finally C ($T_m \approx 155$ K). The initial coverage, determined by integrating the experimental TDS curves, varies over a wide range. For calibration we define here the saturation of peaks A_2 , A_1 and B to correspond to a monolayer coverage of H_2O , $\theta(H_2O) \approx 1$, or 1.1×10^{15} molecules/cm². The justification of this assumption is based on a structural model we propose for a saturated H_2O bilayer on Ni(110) derived from LEED and ESDIAD patterns, which will be discussed in sections 3.2 and 4. Also, the coverage of H_2O in a complete single bilayer on Ru(001) was found to be 1.0×10^{15} molecules/cm² [9].

At the lowest coverage ($\theta(H_2O) \approx 0.06$) only the A_1 and the structured B desorption peaks are observed. With increasing coverage peak A_1 shifts to lower desorption temperature (245 K at $\theta(H_2O) \approx 1$); both peaks A_1 and B increase in intensity and appear to saturate nearly at the same coverage ($\theta(H_2O) \approx 0.5$, curve e, fig. 1). For $\theta(H_2O) > 0.1$ a third peak develops at $T = 210$ K (denoted as A_2) which saturates at $\theta(H_2O) \approx 1$. These data are in substantial agreement with the measurements of Falconer and Madix [18].

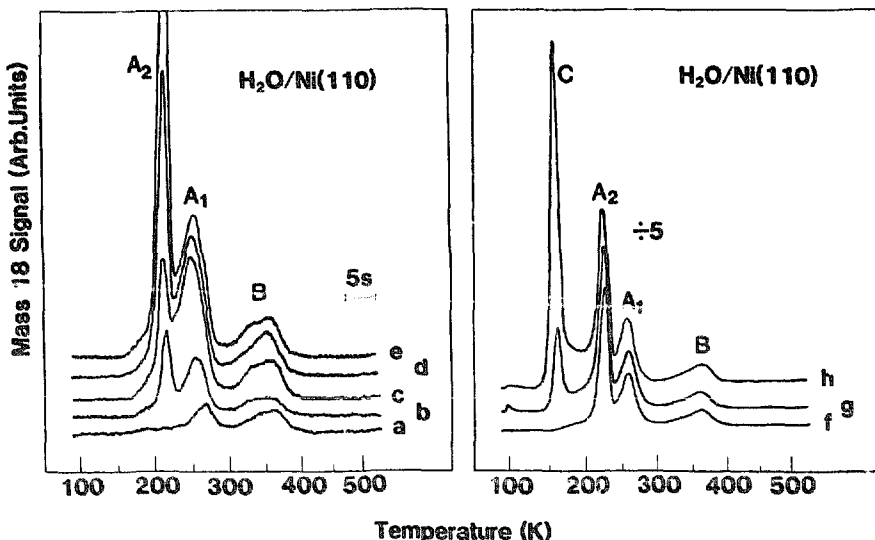


Fig. 1. Mass 18 (H_2O) thermal desorption spectra for H_2O on clean Ni(110). The water coverage for each spectrum is (a) 0.07, (b) 0.14, (c) 0.22, (d) 0.38, (e) 0.50, (f) 0.81, (g) 1.2 and (h) 2.3.

With further increase of H_2O exposure, a relatively sharp desorption peak (C) is formed at $T = 155$ K, which increases monotonically and does not saturate. A similar desorption state has been seen for H_2O on many other surfaces [1], including Ni(111) [2], Ni(100) [3], Ru(001) [9], Pt(111) [10], Ir(110) [28], and Re(001) [16] and has been interpreted as due to ice multilayer desorption.

The sticking coefficient S can be derived from the slope of the coverage versus exposure data; the coverage integrated over all desorption states indicates that the sticking coefficient is nearly independent of $\theta(H_2O)$. In particular, there is no significant change in S during the transition from the submonolayer region to the formation of ice multilayers. Similar conclusions regarding the constancy of S in H_2O adsorption at low temperature have been made for other metal surfaces also [9]. Kurtz et al. recently measured with a calibrated doser system a sticking coefficient $S \approx 1$ for H_2O multilayer adsorption at 80 K [29]. From the constancy of S for H_2O on Ni(110) during the transition from fractional monolayer to multilayers, we conclude that $S \approx 1$ at $\theta(H_2O) \approx 0$ on clean Ni(110).

Based on LEED and ESDIAD experiments described below, we provide interpretations of the relation between the structure of adsorbed H_2O and the TDS data: the A_2 state is suggested to arise from H_2O desorption from a saturated bilayer or from distorted hexagonal H_2O clusters. The A_1 peak is interpreted as desorption from H_2O dimers perhaps stabilized by OH(ad). Finally, the high temperature desorption state B is shown to be due to a recombination of OH(ad) arising from partial dissociation of H_2O on Ni(110).

3.2. ESDIAD and LEED for H_2O on clean Ni(110)

Fig. 2 shows a sequence of ESDIAD and LEED patterns associated with the adsorption of H_2O on Ni(110) at 80 K [20]. Only H^+ ions are observed in ESD of fractional H_2O monolayers, and H^+ dominates in ESD from ice multilayers. At low H_2O coverages ($\theta(H_2O) < 0.2$), where only two peaks A_1 and B were detected in the TDS spectra, a "four-spot" ESDIAD pattern was measured (fig. 2b). The rectangular outline of this four-spot pattern is in registry with the [001] and [110] directions of the LEED pattern (fig. 2a). (As indicated in section 2, the size and shape of this pattern are distorted due to the application of a bias potential between the crystal and the ESDIAD optics; this bias is necessary to compress the ion trajectories so that the entire pattern can be viewed on the phosphor screen.) This four-spot ESDIAD pattern is believed to be due to the existence of H_2O dimers; a structural model based on ESDIAD and angular resolved UPS data, recently published in a short paper [20], will be discussed in section 4.

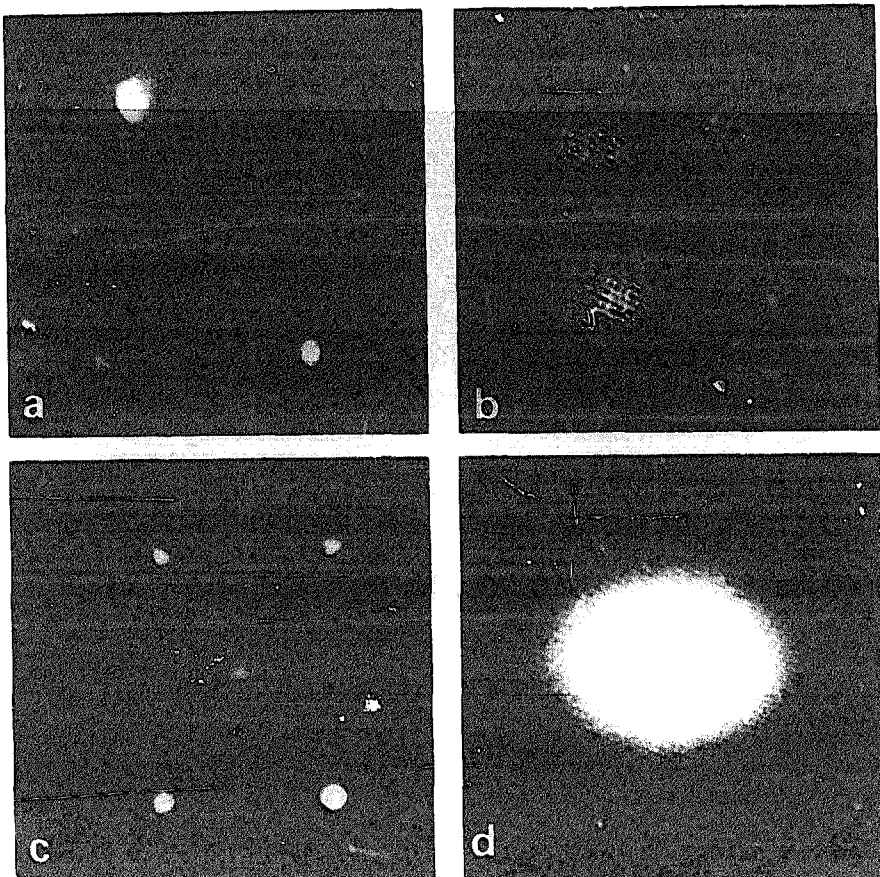


Fig. 2. LEED and H^+ -ESDIAD patterns for H_2O on clean Ni(110). (a) Clean LEED; $E_p = 70$ eV. (b) "Four-spot" ESDIAD pattern for $\theta(H_2O) \approx 0.2$; $E_p = 350$ eV. (c) $c(2 \times 2)$ LEED pattern for $\theta(H_2O) \approx 1$; $E_p = 70$ eV. (d) ESDIAD pattern for $\theta(H_2O) \approx 1$; $E_p = 350$ eV.

We note that the "four-spot" pattern (fig. 2b) actually contains, in addition, two weaker emission spots in [001] surface directions. These additional spots are believed to be due to electron beam damage leading to the formation of OH(ad). As we discuss below, the intensity of these additional spots increases within seconds of electron beam exposure, exceeding even the intensity of the four-spot H_2O dimer pattern.

Normal emission of H^+ is detected in the ESDIAD pattern at higher coverages, related to the observation of peak A, in the TDS. In fig. 2d, the ESDIAD pattern at $\theta(H_2O) > 0.5$ is dominated by a central spot. With further increase of H_2O coverage the central emission spot becomes more intense and broader, without any detectable structure.

At low H_2O coverages with the formation of the four-spot ESDIAD pattern, only diffuse LEED spots from chemisorbed H_2O are observed which

are not reproduced in fig. 2. Fractional order diffraction peaks with slightly varying positions in the [001] direction of the LEED pattern and with half order position in the [110] direction were found for fractional monolayer coverage ($\theta(\text{H}_2\text{O}) < 0.5$). We suggest that both the ESDIAD pattern of fig. 2b and these LEED patterns arise from domains of H₂O dimers with a c(2 × 4) or c(2 × 6) long range order. Evidence for the existence of dimers and a structural analysis will be discussed in section 4.

With increasing coverage a c(2 × 2) LEED pattern is observed over a wide range of H₂O coverage, fig. 2c. At $\theta(\text{H}_2\text{O}) \approx 0.5$ the c(2 × 2) spots are diffuse and dim, but become sharp at $\theta(\text{H}_2\text{O}) \approx 1$. Even for $\theta(\text{H}_2\text{O}) > 1$ the c(2 × 2) pattern is visible, with highly reduced intensity and an increase of the background signal. The same pattern has been observed by Spitzer and Lüth [6] and Bang et al. [5] for H₂O on Cu(110). Bang et al. proposed a model for chemisorbed H₂O in the c(2 × 2) structure, where the H₂O molecules are hydrogen bonded to each other to form a strongly bent and a compressed hexagonal ring structure [5]. Our ESDIAD data for the c(2 × 2) adsorption state on Ni(110) are dominated by normal emission of H⁺ (fig. 2d) and are consistent with this structural model for the c(2 × 2) H₂O layer on Ni(110) which will be discussed in detail in section 4.

We note here that this model derives from the ice H₂O (Ih) "Bilayer" model proposed by DM for H₂O/Ru(001) [9]. On Ru(001), for fractional monolayer coverages, H₂O clusters are formed from H₂O molecules bound directly through the oxygen atom to Ru(001), together with second layer H₂O molecules hydrogen-bonded to first layer H₂O. With increasing coverage, these H₂O clusters grow laterally, forming a continuous H₂O bilayer for $\theta(\text{H}_2\text{O}) = 2/3$. There is an almost perfect match between the hexagonal Ru(001) lattice and the H₂O ice Ih structure, so that the bilayer forms a nearly epitaxial layer. By analogy with the H₂O bilayer structure on Ru(001), the distorted hexagonal structure for H₂O/Ni(110) will be referred to, also, as an H₂O bilayer.

The influence of crystal heating on the ESDIAD pattern of adsorbed H₂O on Ni(110) is demonstrated in fig. 3. The Ni(110) crystal was exposed to H₂O at 80 K, producing a coverage of $\theta(\text{H}_2\text{O}) > 0.5$. The ESDIAD pattern of fig. 3a, with broad intense normal emission, coincides with the observation of the c(2 × 2) LEED structure.

The crystal was successively heated to 160, 200, 250 and 400 K for about 15 s and after cooling down to 80 K, the remaining surface species were probed with ESDIAD (figs. 3b–3d) and LEED. The indicated temperatures of fig. 3, where we observe changes of H⁺ ESDIAD patterns, are lower than the TDS peak temperatures because the onset of H₂O desorption occurs 30–50 K below the peak temperature in TDS. Heating to 160 K for 15 s is accompanied by partial desorption from state A₂ (TDS peak temperature 210 K); due to the decrease of $\theta(\text{H}_2\text{O})$ in the A₂ state, the broad normal emission changes to

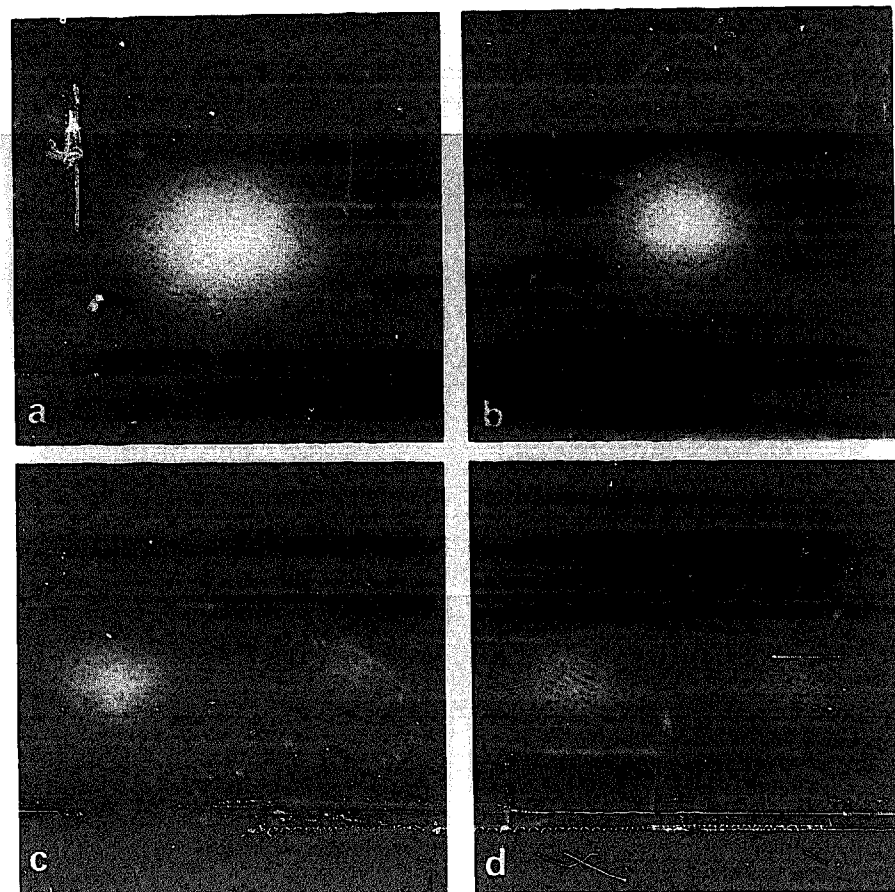


Fig. 3. H^+ ESDIAD patterns for $\theta(H_2O) \approx 0.8$ on clean Ni(110) associated with crystal heating, $E_p = 350$ eV. (a) 80 K, (b) 150 K, (c) 200 K, (d) 250 K.

a sharper central spot (fig. 3b). The second thermal treatment at 200 K leads to further H_2O desorption from the A₂ state. After cooling down we find an ESDIAD pattern with two intense spots in the [001] and [001] directions which are not observed during the adsorption experiments at 80 K. This two-spot pattern is superimposed on the (less intense) four-spot pattern of the low coverage adsorption state. With further increase in temperature, up to 250 K for 15 s, the four-spot pattern disappears, while the two spots in [001] azimuthal directions grow in intensity. This two-spot pattern is characteristic of the species which desorb in the B-state in TDS. Recent angle resolved UPS measurements [23] and high resolution EELS data [30] confirm that OH(ad) is present on the surface after this treatment; the two-spot pattern is related to a partial dissociation of H_2O and the formation of inclined OH(ad) species with azimuthal orientations in [001] or [001] directions [23]. Finally, after heating to 400 K to cause complete desorption from the B-state (recombination of

OH(ad)) the two-spot ESDIAD pattern disappears and no further emission is observed.

In a recent paper [23] we presented evidence that desorption of H₂O at ~ 360 K proceeds via the disproportionation reaction involving recombination of OH(ad), according to



The disproportionation reaction is supported also by our AES data, which show an increase of O(ad) after TDS experiments for successively higher H₂O coverages, since oxygen desorbs from metal surfaces at much higher temperature than water does. As we will demonstrate below, evidence for disproportionation in the presence of predosed oxygen is seen also in isotope exchange experiments involving coadsorption of H₂¹⁶O and ¹⁸O.

The disproportionation reaction is believed to dominate over the recombination reaction,



A similar conclusion was drawn recently for desorption of H₂O from Pd(100) [31]. Moreover, OH formation from dissociation of H₂O should lead to comparable quantities of H(ad). In the absence of the OH + H recombination reaction, therefore, molecular H₂ is expected in TDS experiments due to the recombination of 2H(ad). Unfortunately, this anticipated H₂ desorption following H₂O dissociation on Ni(110) was not probed systematically in the present study.

AES measurements on the Ni(110) sample followed complete desorption of H₂O at 400 K revealed that there was invariably a residual O(KLL) signal whose intensity increased as a function of the initial $\theta(\text{H}_2\text{O})$. Using a calibration method described elsewhere [27], we calculated the residual oxygen coverage after the thermal desorption of ~ 1 monolayer of chemisorbed H₂O to be $\theta(\text{O}) \approx 0.08$. Based on eq. (1) this residual oxygen coverage corresponds to ~ 16% of an H₂O monolayer dissociating into OH(ad). A similar value is derived from the peak area of peak B in the thermal desorption spectra of fig. 1, relative to peaks A₁ + A₂. We cannot eliminate the possibility that a small fraction of the H₂O dissociates completely into O(ad) and H(ad), but believe that formation of OH(ad) is the dominant decomposition process under the present experimental conditions.

We note that the activation barrier for hydrogen abstraction to form OH groups on Ni(110) is on the order of 50 kJ/mol, which is far less than the barrier to breaking an O-H bond in the free water molecule, 500 kJ/mol [1]. The evaluation of the activation barrier for H₂O dissociation on Ni(110) is based on the temperature ~ 200 K at which the formation of OH is evidenced

from ESDIAD; following Thiel and Madey an estimation of the dissociation energy is obtained [1].

3.3. Electron beam-induced surface chemistry

In all of the ESDIAD patterns discussed in the previous section, the total electron dose was sufficiently small for the beam damage to be a minor perturbation (i.e. $< 1 \times 10^{-4} \text{ C/cm}^2$). However, larger electron doses lead to extensive decomposition of chemisorbed H_2O . Fig. 4 shows a series of ESDIAD patterns demonstrating the influence of the electron beam dose. The H_2O -covered Ni(110) crystal was continuously exposed to a 50 nA electron beam ($J_e \approx 3 \times 10^{-5} \text{ A/cm}^2$ at 350 eV) from the ESDIAD electron gun. The

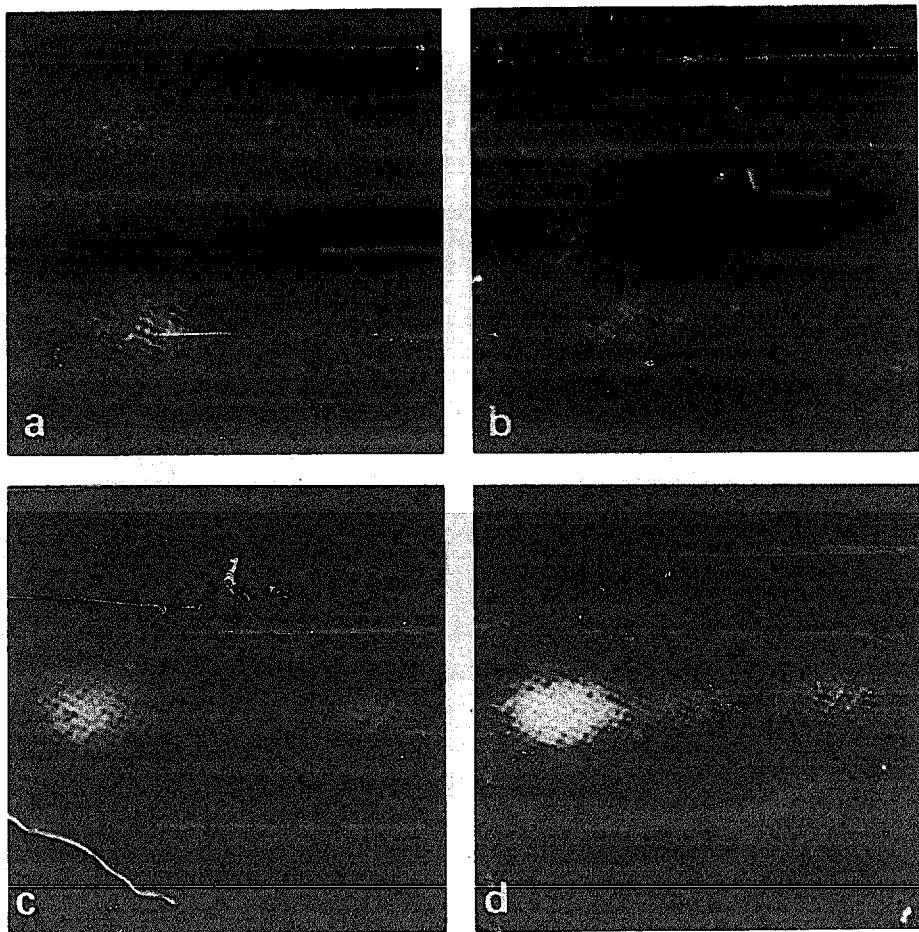


Fig. 4. ESDIAD patterns for $H_2O/Ni(110)$ demonstrating the influence of the electron dose. $J_e \approx 3 \times 10^{-5} \text{ A/cm}^2$ at 350 eV. (a) 0 s, (b) 5 s, (c) 25 s, (d) 120 s.

H^+ ESDIAD patterns of fig. 4 were taken at the beginning of the electron dose (a), or after 5 s (b), 25 s (c) or 120 s (d), respectively. Fig. 4a, with nearly no beam damage, shows the four-spot ESDIAD pattern characteristic of chemisorbed H_2O in the A_1 state. With increasing electron dose two intense spots develop in the [001] and [00 $\bar{1}$] azimuthal directions, apparently due to formation of OH(ad) [23]. In addition, a weaker spot appeared in the direction normal to the surface as the layer became very damaged. At the same time the ESDIAD four-spot pattern from the undamaged chemisorbed layer grew fainter and finally disappeared at an electron dose time of 120 s (fig. 4d). We conclude that beam damage occurs at very small electron beam doses, leading to dissociation of H_2O (ad) mainly into adsorbed OH and H. The cross section for disappearance of the four-spot ESDIAD pattern is $\sim 1 \times 10^{-16} \text{ cm}^2$, comparable to gas phase dissociative ionization cross sections. To minimize electron beam damage in studies of molecular adsorbates as fragile as H_2O on Ni(110), it is essential to keep the electron dose below $\sim 1 \times 10^{-4} \text{ C/cm}^2$ [32].

3.4. Influence of predosed oxygen

3.4.1. Oxygen on clean Ni(110)

Adsorption of the oxygen isotope $^{18}O_2$ at both room temperature and 500 K was followed using AES; the AES O(KLL) intensity versus O_2 exposure measurements were in agreement with previous results [27]. Oxygen adsorbs dissociatively on the Ni(110) surface with an initial sticking coefficient near unity. In accordance with previous data, we observed a (3 \times 1) LEED pattern at 0.2–0.4 L oxygen exposures, followed by a (2 \times 1) pattern at higher exposures (0.7–1.2 L). The calibration of the O(KLL) Auger signal intensity in terms of oxygen coverage was achieved by assuming the (2 \times 1) LEED pattern to correspond to a coverage of $\theta(O) = 0.5$.

Oxide nucleation and growth is observed with further increasing oxygen exposure (> 10 L at 300 K or $> 10^3$ L at 500 K) [33]. In this stage, a preferential growth of oxide islands lateral to the surface occurs, leading to a continuous oxide film with a thickness of about three layers of NiO at saturation ($> 10^4$ L at 500 K) [33]. No LEED pattern is observed from the oxidized Ni(110) crystal.

Most authors agree that the formation of O(2 \times 1) Ni(110) at higher temperature, 500 K, is accompanied by a reconstruction of the Ni(110) surface. Using ion scattering spectroscopy, Van den Berg et al. [34] proposed a “missing row” model in which every second [001] Ni surface row is missing and the oxygen atom is located in long bridge positions between adjacent [110] Ni rows. A recent study of Niehus and Comsa, also with ion scattering spectroscopy, confirmed the “missing row” model for the O(2 \times 1) overlayer

prepared at 450 K [35]. However, at lower adsorption temperature, 300 K, the reconstruction is incomplete and different oxygen adsorption sites seem to be occupied.

Masuda et al. found with HREELS (high resolution electron energy loss spectroscopy) significant changes of the oxygen induced losses from the O(2×1) structure on Ni(110) during thermal annealing from 300 to 450 K [36]. They related these changes to different oxygen positions in the (2×1) structure at 300 and 450 K. At 300 K they proposed for the oxygen adsorption site a short bridge position on top of a [110] surface row of the unreconstructed Ni(110) surface; this model had been proposed previously by Demuth, also [37]. At 450 K, Masuda et al. concluded that a new O(2×1) structure is formed, with the same Ni(110) reconstruction and the same oxygen position suggested by Van den Berg et al. [34].

3.4.2. Influence of O (from fractional monolayer to multilayer oxide) on H_2O adsorption: TDS results

Fractional monolayers of predosed oxygen on Ni(110) dramatically affect subsequent H_2O adsorption–desorption behavior. Fig. 5 shows a sequence of thermal desorption spectra with constant H_2O exposure as a function of preadsorbed oxygen. The constant exposure used in this sequence gave a coverage of $\theta(H_2O) \approx 0.38$, independent of the initial oxygen coverage (i.e., the sticking probability was not influenced by the oxygen). These experiments contain information about (a) the promotion of H_2O dissociation by O(ad), (b) changes in the desorption states A₁ and A₂ from molecularly adsorbed

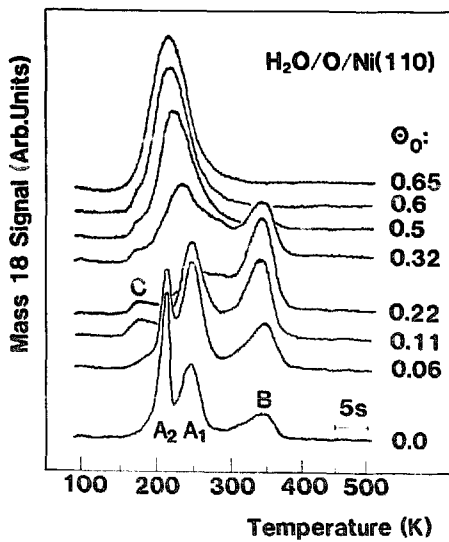


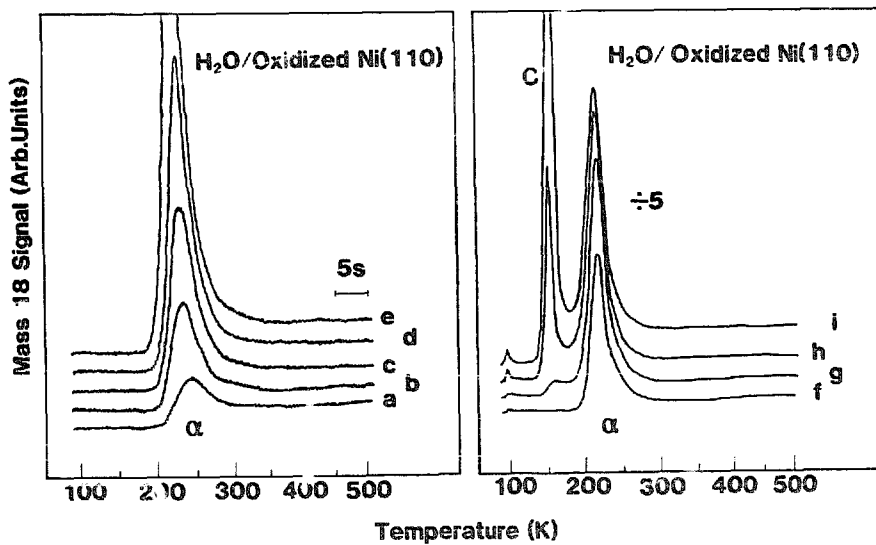
Fig. 5. Mass 18 (H_2O) thermal desorption spectra for $H_2O + O$ on Ni(110); $\theta(H_2O) \approx 0.38$.

water and finally (c) desorption from Ni(110) saturated with chemisorbed O(ad).

(a) With increasing oxygen coverage the desorption peak B (350–360 K) first increases up to $\theta(O) \approx 0.15$ and then decreases with higher oxygen coverage, finally disappearing completely at $\theta(O) \geq 0.65$. The behavior for low oxygen coverage has recently been interpreted as a promotion of H_2O dissociation in the presence of fractional monolayers of O(ad) [23]. The species formed due to this interaction were identified by UPS and ESDIAD to be OH(ad).

(b) A different behavior is found for the desorption peak A_1 (245 K, related to the desorption from H_2O dimers or smaller clusters) and A_2 (210 K, related to the desorption from H_2O bilayers). With even very low oxygen coverage ($\theta(O) \approx 0.06$) the intensity of peak A_2 decreases and nearly disappears at $\theta(O) \approx 0.1$, whereas the desorption peak A_1 first increases up to $\theta(O) \approx 0.22$. With $\theta(O) \approx 0.32$ a new and broad desorption peak develops at a peak temperature of ~ 235 K, shifting with higher oxygen precoverage to 210 K at $\theta(O) \approx 0.65$.

(c) The desorption spectrum from the Ni(110) surface saturated with chemisorbed oxygen ($\theta(O) \approx 0.65$) is completely different from that observed on clean Ni(110): only one broad desorption peak at ~ 210 K is observed from fractional monolayer coverages of H_2O . Desorption peak B from the recombination of OH(ad) is not present for $\theta(O) > 0.6$.



Similar desorption spectra as for $\theta(O) \approx 0.65$ were obtained from Ni(110) oxidized at 500 K ($\sim 10^4$ L oxygen). As mentioned above, oxidation of Ni(110) at 500 K with 10^4 L oxygen leads to a continuous NiO surface layer with ~ 10 Å thickness. H_2O desorption spectra from this oxidized surface are shown in fig. 6. Surprisingly, following the first small H_2O dose ($\theta(H_2O) \approx 0.05$) on the freshly oxidized surface, no H_2O desorption flux could be detected up to 500 K in the TDS spectrum. However, with higher H_2O doses a desorption peak develops with its peak maximum at 245 K (α -state). After the first irreversible adsorption ($\theta(O) \approx 0.05$) the succeeding adsorption and desorption cycles reveal normal behavior: the amount of desorbed H_2O is always equivalent to the dosed H_2O .

The desorption peak for fractional H_2O monolayer coverages from oxidized Ni(110) (fig. 6) shifts with increasing coverage, from 245 to 215 K. Compared to the TDS spectra from the oxygen covered Ni(110) with $\theta(O) \approx 0.65$, the peak width is smaller for H_2O desorbing from oxidized Ni(110). The integrated peak area of desorption peaks α from the oxidized Ni(110) surface is about 20% higher than the peak area of $A_1 + A_2 + B$ from clean Ni(110).

The increase of the H_2O saturation coverage on the oxidized surface is suggested to be due to an increase of the surface roughness during the formation of surface NiO. A further smaller contribution to the increased coverage may arise from the absence of long range ordering within the H_2O layer on oxidized Ni(110).

With further increase of H_2O exposure a second peak develops at 155 K. This peak is observed also on clean Ni(110) for multilayer coverage and can, therefore, be related to the desorption from ice multilayers.

3.4.3. Isotope exchange experiments: $H_2^{16}O + ^{18}O$

The TDS results for the coadsorption of H_2O with small amounts of O(ad) indicate a strong interaction between H_2O (ad) and the modified Ni(110) surface. We suggest that at least two effects contribute to the higher reactivity for hydrogen abstraction. H_2O adsorbed in the neighborhood of O(ad) may, for appropriate spacing between H_2O (ad) and O(ad), form hydrogen bonds which could act as a precursor for H abstraction. A second contribution may arise from the induction of positively charged $Ni^{δ+}$ adsorption sites due to the adsorption of electronegative O [38]. Consequently, the adsorption of H_2O on $Ni^{δ+}$ would allow a larger charge transfer from the adsorbate into the metal, which would strengthen the H_2O -metal bond and weaken the H-O bonds of molecular water [39].

Further information about interactions between H_2O and O(ad) was obtained from isotope exchange experiments. For this purpose the Ni(110) surface was predosed with different $^{18}O_2$ doses and subsequently exposed to $H_2^{16}O$. Isotope mixing (due to hydrogen transfer) between $H_2^{16}O$ and ^{18}O (ad)

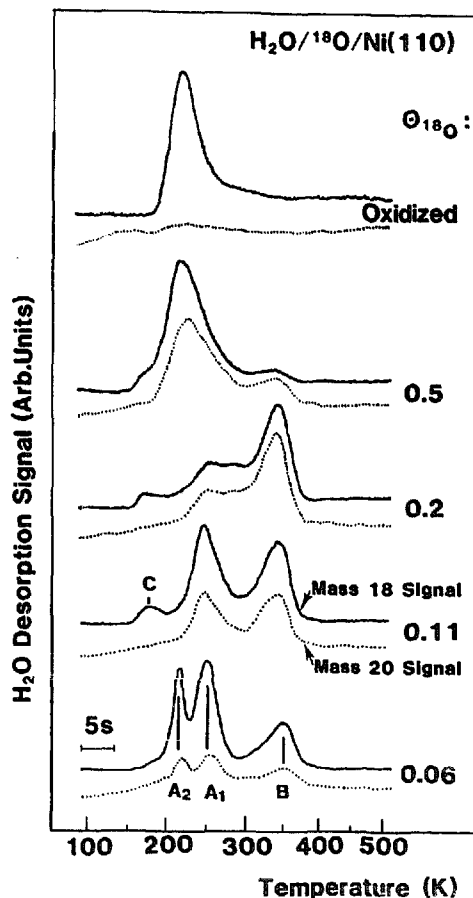


Fig. 7. Thermal desorption spectra for $H_2^{16}O$ adsorbed on ^{18}O -precovered Ni(110); $\theta(H_2O) \approx 0.3$.
Full line: $H_2^{16}O$ mass 18 signal; Dotted line: $H_2^{18}O$ mass 20 signal.

is expected to occur via different pathways: (a) The mobility of protons within hydrogen bonds between chemisorbed $H_2^{16}O$ and ^{18}O may lead to the formation of $H_2^{18}O(\text{ad})$. (b) The formation of $\text{OH}(\text{ad})$ by the reaction of $H_2^{16}O$ with $^{18}O(\text{ad})$ leads to ^{16}OH and ^{18}OH which recombine at higher temperature to form $H_2\text{O(gas)}$ with either mass 18 ($H_2^{16}O$) or mass 20 ($H_2^{18}O$). Fig. 7 shows the experimental TDS results (quadrupole mass 18 signal for $H_2^{16}O$ and mass 20 signal for $H_2^{18}O$) for constant $H_2^{16}O$ dose ($\theta(H_2O) \approx 0.18$) as a function of oxygen ^{18}O preccverage. Our results indicate isotope exchange (hydrogen transfer) for desorption state B (recombination of OH) and even for desorption states A_1 and A_2 , which are believed to be due to molecularly adsorbed H_2O . The intensity ratio of mass 20 ($H_2^{18}O$) to mass 18 ($H_2^{16}O$) desorption flux increases continuously with $\theta(^{18}O)$ reaching ~ 1 for $\theta = 0.5$.

No isotope exchange was observed for H₂O desorption from an ice multi-layer (desorption state C) where the more weakly bonded H₂O is not in direct contact with the ¹⁸O-dosed substrate. Also, no isotope exchange was found for H₂¹⁶O adsorbed on the Ni(110) surface oxidized with ¹⁸O₂ at 500 K, forming a continuous NiO layer. These results indicate quite different behavior for chemisorbed and oxide oxygen.

Our isotope exchange experiments as well as the TDS data presented above (fig. 5) demonstrate that chemisorbed nonlattice oxygen is more reactive in the formation of OH than oxygen from bulk NiO. Our TDS experiments give evidence that the activity of O(ad) for hydrogen abstraction is greatest for low coverage and reaches a maximum for $\theta(O) \approx 0.15$. Geometric site blocking may play a major role for the decrease of reactivity at higher $\theta(O)$ [4]. Carley, Rassias and Roberts [40] suggested that the different reactivity for chemisorbed O(ad) and surface oxide (NiO) reflects the different degrees of coordinative unsaturation between various types of oxygen. Other factors may be operative also [1].

3.4.4. ESDIAD of H₂O + O/Ni(110)

In investigations of adsorbed H₂O it is found using ESDIAD that new bonding configurations can be induced due to interactions between H₂O and O(ad). On Ni(111) for example, Madey and Netzer found evidence for an azimuthal ordering of the water H ligands due to hydrogen bonding to O(ad); no azimuthal ordering could be detected on clean Ni(111) [2]. These results allowed the determination of both H₂O and O(ad) adsorption sites consistent with structural models derived from other techniques.

On Ni(110) the determination of O(ad) adsorption sites is complicated by the reconstruction of the (110) surface induced by chemisorbed oxygen. In the literature, nearly no information for O(ad) adsorption sites is available for low coverages. For higher coverages, with the formation of a (2 × 1) oxygen overlayer, different adsorption sites may be favored for low (300 K) or higher (500 K) preparation temperatures (see section 3.4.1).

The influence of predosed oxygen, $\theta(O) \approx 0.06$, on the ESDIAD patterns for fractional monolayers of H₂O adsorbed at 80 K is demonstrated in fig. 8. It includes the changes observed with ESDIAD during a heating sequence. In this experiment oxygen predosing was performed at 300 K with subsequent annealing to 500 K. The H₂O dose onto the oxygen covered Ni(110) surface corresponded to $\theta(H_2O) \approx 0.1$. On clean Ni(110) this H₂O coverage is associated with a four-spot H⁺ ESDIAD pattern (fig. 2b); instead, on the oxygen dosed surface we detect two intense spots in the [001] and [001] azimuthal directions overlapping with a uniform pattern from H⁺ emission over a wide range of azimuthal and normal directions (fig. 8a). A similar two-spot ESDIAD pattern is observed following thermal decomposition of H₂O (fig. 3d) and due to electron beam damage (fig. 4c), which is related to the formation OH(ad):

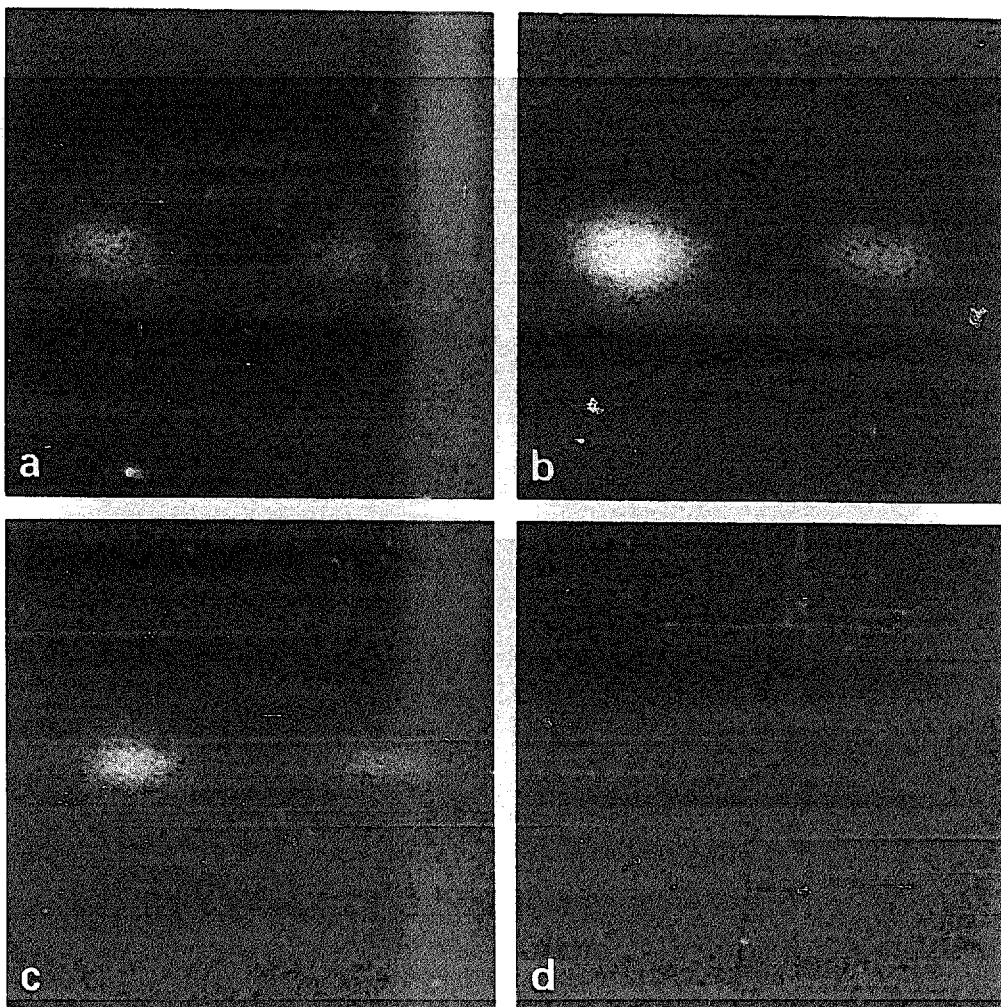
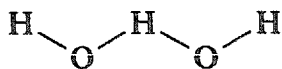


Fig. 8. H^+ ESDIAD patterns for H_2O on oxygen-predosed Ni(110) with $\theta(O) \approx 0.06$ and $\theta(H_2O) \approx 0.1$. (a) 80 K, (b) 140 K, (c) 200 K and (d) 370 K.

the same pattern has been identified using angle resolved UPS as arising from OH(ad) following reaction of H_2O with O(ad) [23]. However, we cannot exclude the possibility that OH groups stabilize H_2O to form linear



complexes which are oriented in the same azimuthal direction as the OH groups and therefore could contribute to the "two-spot" ESDIAD pattern.

With increasing temperature, fig. 8 shows an increase of the intensity of the two spots, accompanied by a decrease of the background emission. This can

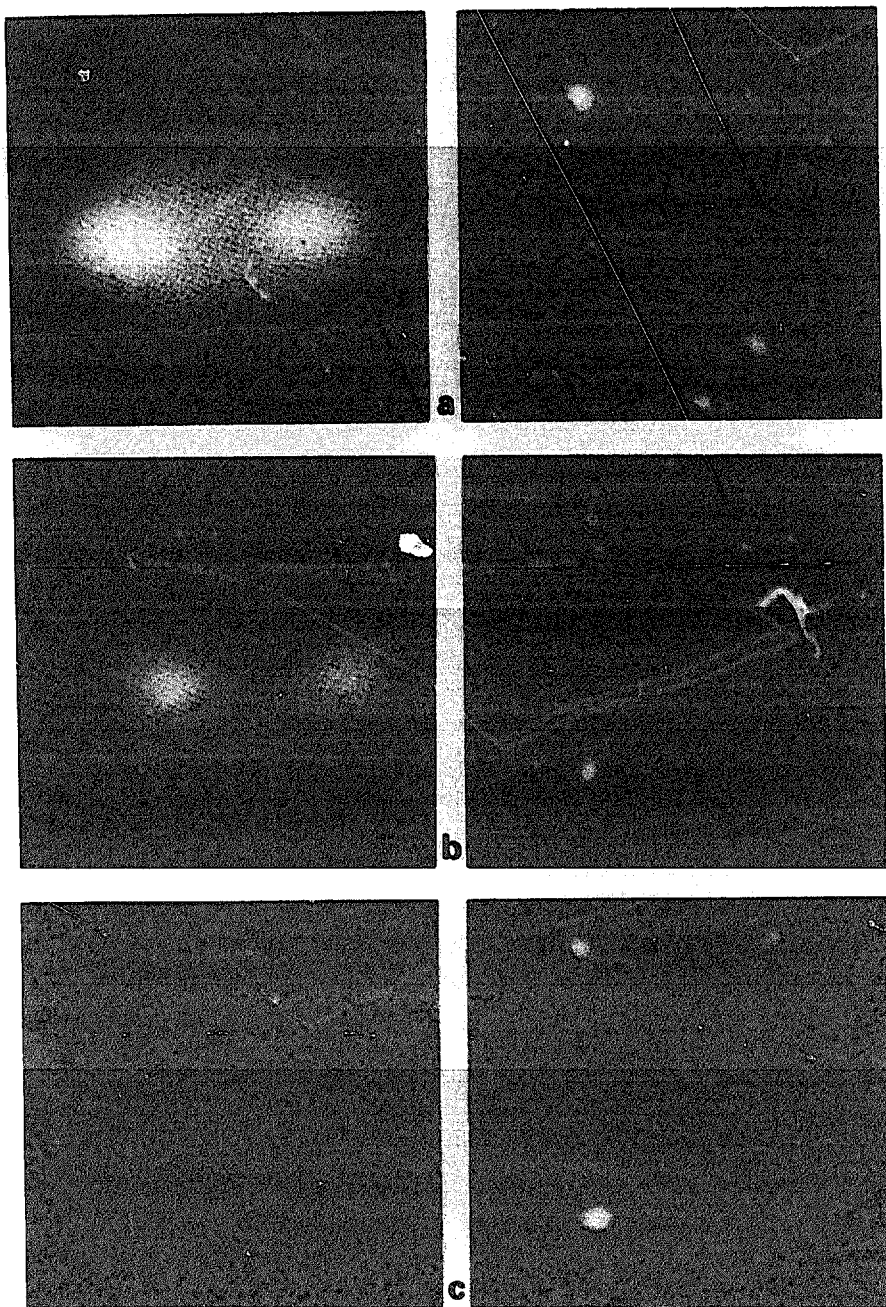


Fig. 9. ESDIAD and LEED patterns for H₂O on oxygen-predosed Ni(110) with $\theta(O) \approx 0.06$; $E_p = 350$ eV for ESDIAD and 70 eV for LEED. (a) ESDIAD and c(2 × 2) LEED; $\theta(H_2O) \approx 0.6$ at 80 K. (b) Changes after heating to 270 K; "Two-spot" ESDIAD and (2 × 1) LEED from surface OH groups. (c) Changes after heating to 370 K; residual ESDIAD and weak O(3 × 1) LEED.

be related to the desorption of molecularly adsorbed H_2O (figs. 8b and 8c). Finally, at $T = 370$ K, where the recombination of OH(ad) and the desorption from peak B is observed with TDS, the two-spot ESDIAD intensity disappears, and only a weak background signal is observed.

In fig. 9 we summarize H^+ ESDIAD and LEED patterns associated with a higher H_2O dose, $\theta(H_2O) \approx 0.6$, onto the oxygen-covered Ni(110) surface which was predosed also with $\theta(O) \approx 0.06$ and annealed to 500 K. The ESDIAD patterns observed during thermal heating are similar to the patterns shown above (fig. 8) for lower $\theta(H_2O)$. At 80 K, both molecularly adsorbed water (broad normal H^+ emission) and OH (two intense H^+ ESDIAD spots along the [001] azimuths) are detected with ESDIAD. Also, the influence of heating is similar to that for lower H_2O coverages: the intensity of the two-spot pattern increases up to 200 K with a simultaneous decrease of the H^+ "background" emission from the desorption of molecularly adsorbed H_2O .

Fig. 9 includes LEED patterns which demonstrate that the adsorption of H_2O onto the oxygen dosed Ni(110) followed by thermal heating is associated with the observation of a new LEED overlayer which was not observed for H_2O alone on clean Ni(110). For example, an oxygen dose of $\theta(O) \approx 0.06$ followed by annealing to 500 K led to a faint (3×1) LEED pattern with streaks of the 1/3 order spots in $[1\bar{1}0]$ directions. Dosing of $\theta(H_2O) \approx 0.6$ at 80 K changed the LEED to a $c(2 \times 2)$ overlayer, which has also been found for $\theta(H_2O) = 0.5-1$ on clean Ni(110). During thermal heating, the $c(2 \times 2)$ overlayer from $H_2O + O$ changed between 200 and 270 K into a (2×1) LEED pattern and finally for temperatures higher than 370 K back to the faint (3×1) overlayer from O(ad). These structural changes are consistent with our TDS and ESDIAD data. Heating to 270 K led to the desorption of molecularly adsorbed H_2O (desorption of states $A_1 + A_2$); in the same temperature range, 200–270 K, the two-spot H^+ ESDIAD pattern from OH groups became most intense, fig. 8c. Therefore, we conclude that the intermediate (2×1) LEED pattern is associated with OH(ad). The same LEED pattern was observed recently for the coadsorption of $H_2O + O$ on Ni(110) at 250 K; in these experiments the OH(ad) product was identified by UPS [23]. The orientation of the OH groups within the (2×1) overlayer from $H_2O + O$ could be determined with ESDIAD and UPS. However, we do not have any information to indicate whether or not this overlayer is associated with a reconstruction of Ni(110), as seen for the O(2×1) overlayer on Ni(110).

Finally we studied H_2O adsorption on the O(2×1) structures prepared at both 300 and 500 K with ESDIAD. The results for the differently prepared O(2×1) Ni(110) surfaces, however, show no significant differences in the sequence of ESDIAD patterns from H_2O adsorbed at 80 K. Fig. 10 shows, for example, the LEED and ESDIAD patterns associated with H_2O on the

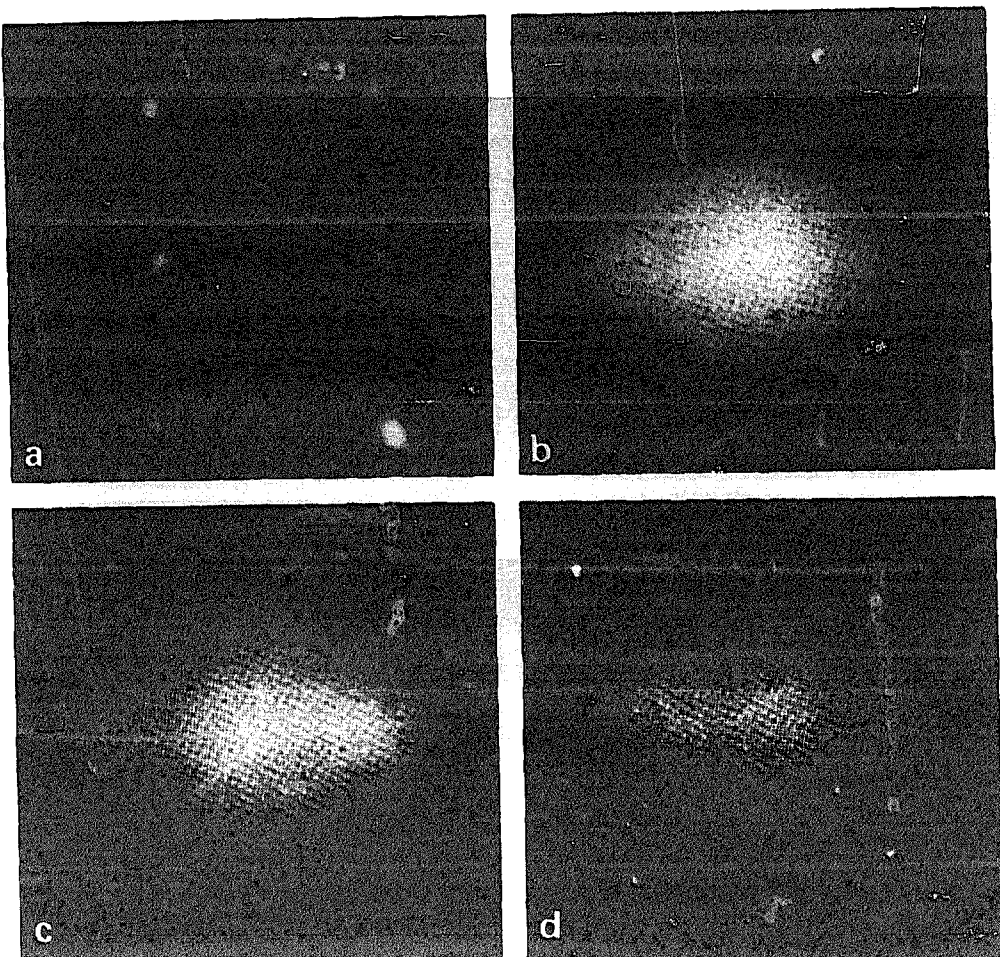


Fig. 10. LEED and ESDIAD for H_2O adsorbed on $O(2 \times 1)$ Ni(110) prepared at 500 K. (a) LEED $O(2 \times 1)$; $E_p = 70$ eV. (b) ESDIAD for $\theta(H_2O) \approx 0.06$ on $O(2 \times 1)$ Ni(110) at 80 K. (c), (d) Changes of ESDIAD patterns after heating to 200 and 350 K, respectively.

$O(2 \times 1)$ overlayer annealed to 500 K. This oxygen overlayer shows a sharp (2×1) LEED pattern (fig. 10a). After dosing $\theta(H_2O) \approx 0.07$ at 80 K we observe the ESDIAD circular emission in directions normal to the surface, with some preferential emission for large angles in [001] azimuths (fig. 10b). Heating the crystal to 200 and 350 K is associated with further increase of the asymmetry of the ESDIAD pattern (figs. 10c and 10d). Despite the brightness of the photos of fig. 10, the total emission intensity is much less than observed for lower oxygen precoverages, when more OH(ad) is formed. (cf. figs. 5 and 8). Above 350 K, due to the final desorption of H_2O from OH groups, the H^+ emission vanishes. For the adsorption of H_2O on $O(2 \times 1)$ Ni(110) no new LEED overlayers were observed.

The reconstructed O(2×1) Ni(110) surface exhibits relatively deep troughs in [001] surface directions. Therefore, the adsorption sites we proposed for the oriented H_2O dimer species at low coverage on clean Ni(110) or for OH groups from $H_2O + O$ (see section 4) are no longer existent or are occupied by O(ad). The nearly circular H^+ emission at 80 K suggests an H_2O adsorption configuration on O(2×1) Ni(110) with little preferential azimuthal orientation of the H ligands. The greater asymmetry of the ESDIAD patterns for 200 and 350 K is related to the desorption of molecular water and to the formation of OH groups. We note that the symmetry of the H^+ emission is in the same direction as the orientation of the troughs from the reconstructed O(2×1) Ni(110). At higher temperature (350 K), where we believe that molecular H_2O is not stable at the surface, the H^+ ESDIAD pattern (fig. 9d) suggests traces of OH species oriented perpendicular as well as inclined to the surface with a preferential orientation in [001] azimuths.

4. Discussion

In this section we first discuss the molecular adsorption of H_2O on clean Ni(110) and compare its behavior with other H_2O /metal systems. Also, we briefly discuss the recently proposed H_2O dimer cluster and bilayer configurations on Ni(110), which are based on ESDIAD, LEED and ARUPS results. In the second part we focus on the influence of surface oxygen on the adsorption, orientation and dissociation of $H_2O/Ni(110)$. The discussion for $H_2O + O/Ni(110)$ includes the different behavior of low coverage "chemisorbed" oxygen and high coverage oxide oxygen.

For H_2O adsorption on Ni(110) we can conclude from ESDIAD and TDS data that both molecular and dissociative adsorption exist on clean Ni(110). At low temperature (80–200 K) H_2O adsorbs molecularly on Ni(110); with increasing crystal temperature ($T > 200$ K) a fraction of the H_2O (ad) dissociates. The influence of surface oxygen on H_2O adsorption and desorption behavior is rather complex. The dissociation of H_2O is found to be promoted by surface oxygen even at 80 K. Insight into the oxygen-induced dissociation of H_2O is gained from isotope exchange experiments with ^{18}O (ad).

4.1. Molecular adsorption of H_2O on clean Ni(110)

Detailed information about the molecular structure of H_2O on transition metals, including Ni(111) [2], Ru(001) [9] and Re(001) [16], has been obtained using ESDIAD. A common result of these previous studies and of the present ESDIAD study is that the only detectable ion in ESD for fractional H_2O

monolayers is H^+ . This result is consistent with a model in which H_2O is bound via the oxygen atom to the metal with the H ligands pointing away from the substrate. This orientation of H_2O on transition metals is supported by EELS measurements in which both H-bonded and non-H-bonded OH vibrations are seen, and by work function measurements, $\Delta\phi$, which show a work function decrease upon H_2O adsorption on several transition metals [4–6]. The decrease of ϕ is consistent with an H_2O orientation where the negative end of the H_2O dipole, the O atom, is directed towards the substrate while the positive end (H) points away from the surface.

The interpretation of ESDIAD patterns in this and in previous publications is based on the fact that the direction of H^+ emission from $H_2O(\text{ad})$ is determined by the direction of O–H bonds which are ruptured by electronic excitations. As demonstrated by DM [9], ESDIAD patterns allow the determination of different H_2O adsorption species; for $H_2O/\text{Ru}(001)$, DM detected H_2O monomers or disordered clusters at low coverages. For higher H_2O coverage, the formation of larger hydrogen bonded H_2O clusters with orientations in registry with the substrate was observed [9].

For fractional monolayer coverage of $H_2O/\text{Ni}(100)$ we present two different H^+ ESDIAD patterns (fig. 2). In combination with LEED and ARUPS, these ESDIAD data allow us to formulate models of H_2O orientation in hydrogen bonded clusters.

In fig. 11 we briefly summarize structural models which we recently proposed for molecular adsorbed H_2O on $\text{Ni}(110)$ [20]. For low H_2O coverages ($\theta(H_2O) < 0.5$), where ESDIAD shows a “four-spot” pattern (fig. 2b), we propose the formation of oriented H_2O dimer clusters, fig. 11a. In this model, each dimer is made up of two H_2O molecules hydrogen bonded to each other. Within the O–H \cdots O bond, one H_2O molecule acts as a proton donor, the other as a proton acceptor. Due to the different contribution to the hydrogen bond, the $1b_1$, $3a_1$, and $1b_2$ H_2O molecular orbitals split into two energetically separated sets of orbitals from proton donor and proton acceptor H_2O [20]. Therefore, the existence of H_2O dimers can be evidenced from UPS, which shows a “six-peak” spectrum for $H_2O/\text{Ni}(110)$ for $\theta(H_2O) < 0.5$ [20]. The azimuthal orientation of the H_2O dimer proposed in fig. 11a, with the O–H \cdots O axis along [001] azimuths, is based on ESDIAD and ARUPS results. In the proposed structure, three H atoms and one oxygen lone pair from the H donor molecule are pointing away from the surface. These four directions are active for H^+ ESD emission. The direction of the oxygen lone pair orbital becomes equivalent to an H^+ active O–H direction by rotating the dimer by 180° . If we assume that the azimuthal directions of H^+ emission in the ESDIAD experiment are determined by the O–H bond directions, a four-spot ESDIAD pattern is expected. This is in accordance with the experimental results, fig. 2b.

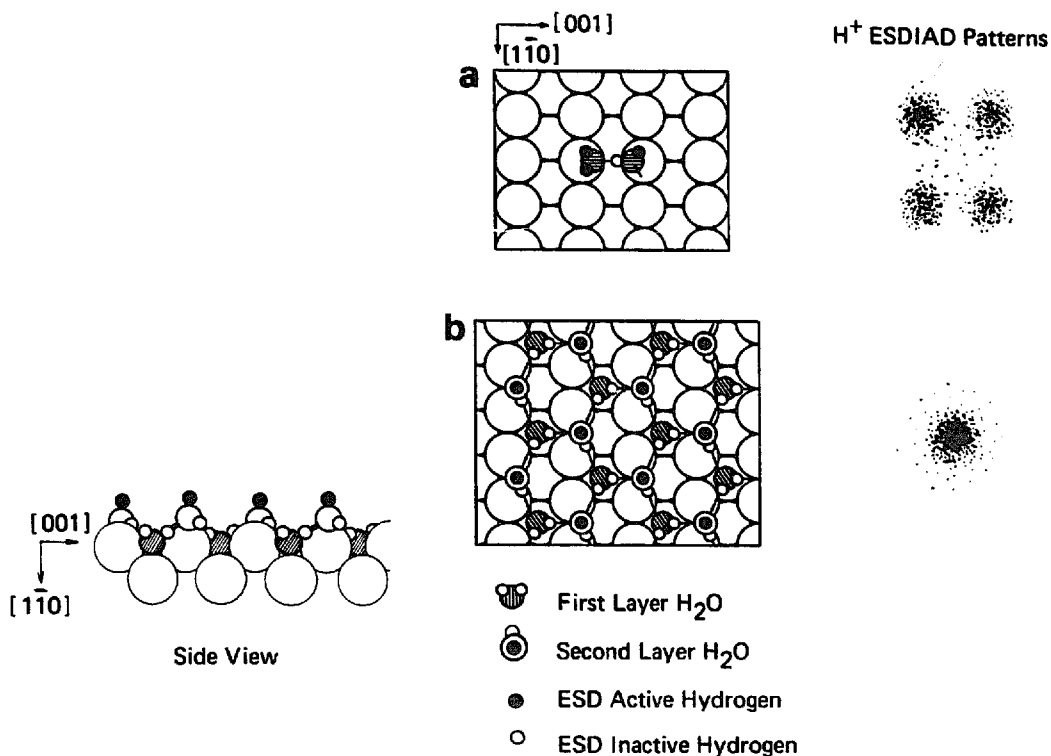


Fig. 11. Structural models for H_2O adsorbed at 80 K on Ni(110) based on ESDIAD, LEED and recent UPS [20] measurements. (a) H_2O dimer formation for $\theta(H_2O) < 0.5$. (b) Distorted hexagonal H_2O bilayer for $\theta(H_2O) = 1$.

For higher water coverages, $\theta(H_2O) = 0.5\text{--}1$, we propose the formation of larger hydrogen bonded clusters with H_2O molecules arranged in a distorted hexagonal bilayer, fig. 11b. The proposed model is consistent with LEED and ESDIAD as well as with ARUPS [20] measurements. The structural model shows a $c(2 \times 2)$ long range order, which was detected with LEED for $\theta(H_2O) = 0.5\text{--}1$. ESD-active H ligands are found for “second-layer” H_2O molecules with “flip-up” [9] configurations; the O–H bond is directed normal to the surface consistent with the normal H^+ emission observed with ESDIAD (fig. 2d).

In accordance with the distorted hexagonal bilayer model, fig. 11b, UPS measurements show that the splitting of the $1b_1$, $3a_1$ and $2b_2$ orbitals into the “six-peak” spectrum of H_2O dimers at low H_2O coverages vanishes for $\theta(H_2O) = 0.5\text{--}1$. In the hexagonal bilayer structure, fig. 11b, each H_2O molecule acts as H-donor and H-acceptor molecule at the same time and the splitting of the $1b_1$, $3a_1$ and $1b_2$ from H-donor and H-acceptor molecules can no longer be separated with UPS [20].

The existence of H_2O dimers has not been reported previously for other H_2O /transition metal surfaces. However, Schmeisser et al. reported the existence of H_2O dimers [41] on UN and interpreted their data in terms of theoretical calculations of H_2O dimers by Umeyama and Morokuma [42]. On Ni(110) we believe that the stability of H_2O dimer clusters is due to a moderately strong interaction between H_2O and the Ni substrate and to a good match of the O–H \cdots O distance of the dimer (2.98 Å [43]) and the Ni–Ni distance (3.52 Å) between surface rows of Ni atoms on Ni(110). However, a stabilization of the H_2O dimers on Ni(110) by OH from partial dissociation cannot be ruled out completely. The observation of weak LEED patterns for $\theta(H_2O) < 0.5$ suggests a short range repulsive interaction between the H_2O dimers which inhibits at lower coverages, also, the formation of larger clusters. Only when the surface becomes highly crowded with H_2O the short range attractive interaction once more dominates, and the net energy is further lowered due to the formation of a hydrogen-bonded bilayer network.

The formation of hexagonal bilayer ring clusters of hydrogen bonded H_2O had been previously proposed by DM for $H_2O/Ru(001)$ [9] and for $H_2O/Cu(110)$ by Bange et al. [5]. On the close packed hcp Ru(001) surface a nearly perfect match between the substrate spacing and a hexagonal H_2O bilayer of a unit cell size derived from ice structures is achieved. On Ni(110) the hexagonal bilayer has to be compressed in [001] and to be strained in [110] azimuthal directions to match the substrate distances and to achieve a c(2 × 2) long range order. This, we believe, is a further reason why dimers form at lower H_2O coverages, for $\theta(H_2O) < 0.5$.

The TDS of H_2O on Ni(111), Ni(100), and Ni(110) display evidence for a remarkable structural specificity in adsorption of H_2O on Ni surfaces. On Ni(111) and Ni(100), only molecular adsorption is seen; adsorption–desorption of H_2O is reversible, with no evidence for dissociation. In contrast, on Ni(110), adsorption of H_2O at 80 K leads, upon heating, to an activated decomposition of a fraction of the H_2O monolayer. Moreover, the binding energy of molecular H_2O to Ni(110) is considerably stronger than on Ni(100) and Ni(111).

Our TDS results demonstrate that the H_2O –Ni(110) bond is moderately strong, compared to Ni(111), Ni(110) and to other H_2O /transition metal systems. For comparison we choose the temperature separation ΔT between the desorption peak temperatures for fractional monolayer coverages and the multilayer desorption peak. Of course, the exact temperature position of a TDS peak may depend on experimental conditions as, for example, the heating rate and on different frequency factors for different H_2O desorption states. With the measurement of ΔT some of these uncertainties are suppressed.

For $H_2O/Ni(110)$ the desorption states A_1 and A_2 are separated by $\Delta T \approx 105$ and ≈ 45 K from the multilayer desorption state, which was found

in the present work at 165 K. On other Ni single crystal surfaces, the H_2O -Ni bond is weaker. On both Ni(111) and Ni(100), only one desorption state is observed for fractional monolayer coverages with $\Delta T \approx 15-20$ K [Ni(111)] or $\Delta T \approx 15$ K [Ni(100)]. On Ni(100), however, some traces of H_2O desorb up to $\Delta T \approx 65$ K. Higher desorption temperatures have been reported for $H_2O/Ru(001)$, where two desorption states, denoted as A_1 with $\Delta T \approx 65$ K and A_2 with $\Delta T \approx 25$ K, were detected [9] and for $H_2O/Re(001)$ with $\Delta T \approx 40$ and 10 K [16]. A very weak interaction between $H_2O(ad)$ and the substrate is found on Ag surfaces of different orientation, where no separation between the desorption temperature for fractional monolayer coverages and multilayer coverages is found [14,15].

The interpretation of the desorption states A_1 and A_2 for Ni(110) is based on the different structural models proposed for $\theta(H_2O) < 0.5$ and $\theta(H_2O) \approx 0.5-1$, fig. 11. Desorption state A_2 with $\Delta T \approx 45$ K is suggested to arise from the desorption of H_2O from larger H_2O bilayer clusters. During the desorption from the A_2 state, the hexagonal ring clusters break into smaller more stable clusters which have been identified with ESDIAD and ARUPS [20] as H_2O dimers. These dimer clusters desorb in the A_1 desorption state with $\Delta T \approx 105$ K, accompanied by partial dissociation into $OH(ad)$ and $H(ad)$. However, we cannot exclude that the high desorption temperature of the A_1 state is associated with a stabilization of H_2O by $OH(ad)$. Molecular orbital cluster calculations by Kühnholz and Grodzicki [44] for a H_2O dimer in the same orientation as proposed in fig. 11a suggests that the total energy minimum of the $(H_2O)_2/Ni(110)$ cluster is associated with a considerable movement of the proton within the hydrogen bond $O \cdots HO$ of the dimer, towards the oxygen atom of the H-acceptor H_2O . These calculations reproduce quite well the observed experimental splitting of molecular orbitals from H-donor and H-acceptor molecules. The resulting configuration $H_2OH \cdots OH$ of the H_2O dimer can be interpreted as a precursor state for H_2O dissociation. We note that a similar sequence of desorption states due to breaking of hexagonal ring clusters, the possible existence of oriented H_2O dimers, and finally desorption of H_2O from dimers with partial dissociation have been proposed by Jupille et al. for $H_2O/Re(001)$ [16]. However, there is a striking difference between $H_2O/Ni(110)$ and $H_2O/Re(001)$. The dissociation observed on both metals is associated with the formation of OH . On Ni(110), OH recombines to form H_2O which desorbs at 350–370 K whereas on Re(001) there is evidence for further dissociation of OH into $H + O(ad)$ for $T > 360$ K [16].

4.2. Influence of $O(ad)$

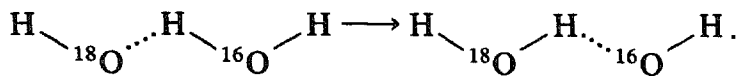
For coadsorption of H_2O and low oxygen precoverages we find clear evidence for a promotion of H_2O dissociation with the formation of oriented

OH species on Ni(110). The dissociation of H_2O , which occurs partially on clean Ni(110) above 200 K, is believed to occur for O + Ni(110) already at 80 K. We conclude that the reactivity of Ni(110) for OH formation from adsorbed H_2O molecules is further increased by O(ad). The behavior of $H_2O + O/Ni(110)$ is to some extent similar to that of $D_2O + O$ on Ni(100) [3]. On Ni(100), also, the population of a high temperature desorption state increases for low oxygen coverages with increasing $\theta(O)$; on this surface, the formation of a cooperative sorption complex $(OD)_2D_2O$ was postulated from UPS and XPS [3]. The behavior on Ni(111) is to some extent different. Madey and Netzer [2] found for $H_2O + O$ new desorption states with higher desorption temperature, which they relate to attractive hydrogen bonding interactions. From ESDIAD patterns they postulated the formation of intermediate OH species. However, recent UPS, XPS and isotope exchange experiments with ^{18}O (ad) revealed within the detection limit of photoelectron spectroscopy no hints for the formation of OH(ad) or isotopic exchange for O + Ni(111) [45]. We conclude that the different crystallographic orientations play an important role for $H_2O + O$ interaction and reaction on Ni surfaces.

Our present isotope exchange experiments for $H_2^{16}O + ^{18}O$ as well as LEED data confirm the formation of cooperative sorption complexes between $H_2^{16}O$ and ^{18}O or $H^{18}O$ on Ni(110). For the formation of mass 20 water molecules ($H_2^{18}O$) from $H_2^{16}O + ^{18}O$, two H atoms within hydrogen bonds have to be transferred from $H_2^{16}O$ to ^{18}O . In a simple picture, the formation of $H_2^{18}O$ can be described by a hydrogen bond interaction between two $H_2^{16}O$ and one ^{18}O



or for one $H_2^{16}O$ and one ^{18}OH species:



This interpretation is based on the mobility of the hydrogen atom within the hydrogen bonds, which is reported to occur readily in solid ice [46], although isotopic mixing was *not* seen in TDS during desorption from $D_2O + H_2O$ multilayers adsorbed on Ru(001) [8].

LEED experiments for $H_2O + O$, fig. 8, are in accordance with the idea of cooperative sorption complexes between H_2O , OH and O. Starting with a (3×1) overlayer from O(ad), for example, we observed a change to the c(2×2) structure after dosing H_2O with $\theta(H_2O) \approx 0.5-1$. This result gives evidence for the incorporation of O(ad) or OH(ad) into the hexagonal bilayer

cluster, fig. 11b. The LEED scattering cross section for OH and H_2O should be nearly the same, provided that the adsorption sites are identical. Also, the change from the $c(2 \times 2)$ pattern into the (2×1) after annealing to 200–270 K shows that O(ad) is incorporated into the sorption complex formed by OH(ad) and O(ad) species.

5. Conclusion

We briefly summarize the main conclusions which result from our data for H_2O on clean and oxygen-dosed Ni(110).

(1) H_2O adsorbs molecularly at 80 K on clean Ni(110) at all coverages. At higher temperatures, > 200 K, a “two-spot” ESDIAD pattern, which has recently been identified to be due to oriented OH groups, gives evidence for a partial dissociation of H_2O (ad) into OH and H. The relatively high TDS desorption temperature for $H_2O/Ni(110)$ – compared to Ni(100) and Ni(111) – is suggested to be due to the local atomic roughness of the Ni(110) surface allowing the formation of oriented dimer clusters and to a stabilizing effect of OH formed above 200 K.

(2) Adsorption of fractional monolayer H_2O on Ni(110) at 80 K is associated with the formation of hydrogen bonded clusters showing short range as well as long range ordering. A “four-spot” ESDIAD pattern observed for $\theta < 0.5$ at 80 K suggests the existence of oriented H_2O dimer clusters containing one H-donor and one H-acceptor molecule; the existence of H_2O dimer clusters on Ni(110) has also been identified recently by the splitting of the H_2O molecular orbitals in UPS. The existence of ordered LEED structures indicates that there is a short-range repulsive interaction between dimers which prevents the formation of larger hydrogen-bonded clusters, but a longer range attractive interaction which results in ordered LEED structures. At higher H_2O coverages, $\theta(H_2O) = 0.5–1$, some H_2O molecules are forced into second layer adsorption sites and the existence of distorted hexagonal ring clusters with a $c(2 \times 2)$ long range symmetry is postulated from LEED and ESDIAD.

(3) Surface oxygen promotes even at 80 K the dissociation of H_2O into OH and H. Above 200 K, cooperative sorption complexes form from $H_2O + O$ coadsorption due to the formation of OH and due to strong lateral attractive interaction (including hydrogen bonding) between H_2O , OH and O; in a limited regime of coadsorption coverages, $H_2O + OH + O$, a (2×1) long range order occurs. The existence of sharp (2×1) overlayer spots in LEED is consistent with the interpretation that the adsorption sites of H_2O , OH and O in this surface complex are identical.

(4) The adsorption experiments on clean Ni(110) suggest that the activation barrier to breaking an O–H bond, which is for a free water molecule ~ 500 kJ/mol, is lowered to ~ 50 kJ/mol on clean Ni(110); this barrier is further lowered by preadsorbed O(ad) to < 20 kJ/mol. Insights into the dissociation pathway were gained from isotope exchange experiments with predosed ¹⁸O(ad) and adsorbed H₂¹⁶O revealing a high proton mobility within hydrogen bonds between H₂O and O.

Acknowledgements

Financial support by the Deutsche Forschungsgemeinschaft and by a NATO research grant is gratefully acknowledged. This work was also supported in part by the US Department of Energy, Division of Basic Energy Sciences.

References

- [1] P.A. Thiel and T.E. Madey, Surface Sci. Rept. 7 (1987) 211.
- [2] T.E. Madey and F.P. Netzer, Surface Sci. 117 (1982) 549.
- [3] D.E. Peebles and J.M. White, Surface Sci. 144 (1984) 512.
- [4] C. Benndorf, C. Nöbl, M. Rüsenerg and F. Thieme, Surface Sci. 111 (1981) 87.
- [5] K. Bange, D.E. Grider, J.K. Sass and T.E. Madey, Surface Sci. 137 (1984) 38.
- [6] A. Spitzer and H. Lüth, Surface Sci. 120 (1982) 376.
- [7] T.E. Madey and J.T. Yates, Jr., Chem. Phys. Letters 51 (1977) 77;
T.E. Madey and J.T. Yates, Jr., in: Proc. 7th Intern. Vacuum Congr. and 3rd Intern. Conf. on Solid Surfaces, Eds. R. Dobrozemsky et al. (Burger, Vienna, 1977) p. 1183.
- [8] P.A. Thiel, F.M. Hoffmann and W.H. Weinberg, J. Chem. Phys. 75 (1981) 5556.
- [9] D.L. Doering and T.E. Madey, Surface Sci. 123 (1982) 305.
- [10] G.B. Fisher and J.L. Gland, Surface Sci. 94 (1980) 446.
- [11] B.A. Sexton, Surface Sci. 94 (1980) 435.
- [12] H. Ibach and S. Lehwald, Surface Sci. 91 (1980) 187.
- [13] E. Stuve, R.J. Madix and B.A. Sexton, Surface Sci. 111 (1981) 11.
- [14] S.T. Ceyer and J.T. Yates, Jr., to be published.
- [15] M. Klaua and T.E. Madey, Surface Sci. 136 (1984) 142.
- [16] J. Jupille, P. Pareja and J. Fusy, Surface Sci. 139 (1984) 505.
- [17] P.A. Thiel, F.M. Hoffmann and W.H. Weinberg, Phys. Rev. Letters 49 (1982) 501.
- [18] J.L. Falconer and R.J. Madix, J. Catalysis 51 (1978) 47.
- [19] J.D. Bernal and R.H. Fowler, J. Chem. Phys. 1 (1933) 515;
L. Pauling, J. Am. Chem. Soc. 57 (1935) 2680.
- [20] C. Nöbl, C. Benndorf and T.E. Madey, Surface Sci. 157 (1985) 29.
- [21] F.P. Netzer and T.E. Madey, Phys. Rev. Letters 47 (1981) 928.
- [22] D.L. Doering, S. Semancik and T.E. Madey, Surface Sci. 133 (1983) 49.
- [23] C. Benndorf, C. Nöbl and T.E. Madey, Surface Sci. 138 (1984) 292.
- [24] T.E. Madey and J.T. Yates, Jr., Surface Sci. 63 (1977) 203.

- [25] D.L. Doering and S. Semancik, *Surface Sci.* 129 (1983) 177.
- [26] T.E. Madey, in: *Inelastic Particle-Surface Collisions*, Ed. E. Taglauer and W. Heiland (Springer, Berlin, 1981).
- [27] C. Benndorf, B. Egert, C. Nöbl, H. Seidel and F. Thieme, *Surface Sci.* 92 (1980) 636.
- [28] T.S. Wittrig, D.E. Ibbotson and W.H. Weinberg, *Surface Sci.* 102 (1981) 506.
- [29] R.L. Kurtz, N. Usuki, R. Stockbauer and T.E. Madey, *J. Electron Spectrosc. Related Phenomena* 40 (1986) 35.
- [30] L. Ollé, M. Salmerón and A.M. Baró, *J. Vacuum Sci. Technol.* A3 (1985) 1866.
- [31] E.M. Stuve, S.W. Jorgensen and R.J. Madix, *Surface Sci.* 146 (1984) 179.
- [32] C.G. Pantano and T.E. Madey, *Appl. Surface Sci.* 7 (1981) 115.
- [33] D.F. Mitchell, P.B. Sewell and M. Cohen, *Surface Sci.* 69 (1977) 310.
- [34] J.A. Van den Berg, L.K. Verheij and D.G. Armour, *Surface Sci.* 91 (1980) 218.
- [35] H. Niehus and G. Comsa, *Surface Sci.* 151 (1985) L171.
- [36] S. Masuda, M. Nishijima, Y. Sakisaka and M. Onchi, *Phys. Rev. B25* (1982) 863.
- [37] J. Demuth, *J. Colloid Interface Sci.* 58 (1977) 184.
- [38] P.C. Stair, *J. Am. Chem. Soc.* 104 (1982) 4044.
- [39] J.E. Müller, *Surface Sci.* 178 (1986) 589.
- [40] A.F. Carley, S. Rassias and M.W. Roberts, *Surface Sci.* 135 (1983) 35.
- [41] D. Schmeisser, F.J. Himpsel, G. Hollinger and B. Reihl, *Phys. Rev. B27* (1983) 3279.
- [42] H. Umeyama and K. Morokuma, *J. Am. Chem. Soc.* 99 (1977) 1316.
- [43] M.D. Newton and N.R. Kestner, *Chem. Phys. Letters* 94 (1975) 501.
- [44] O. Kühnholz and M. Grodzicki, *J. Mol. Struct.*, in press.
- [45] C. Nöbl and C. Benndorf, *Surface Sci.* 182 (1987) 499.
- [46] P. Schuster, in: "The Hydrogen Bond", Eds. P. Schuster, G. Zundel and C. Sandorfy (North-Holland, Amsterdam, 1976) p. 27.